ARTICLE

Mutations in the Cilia Gene *ARL13B* Lead to the Classical Form of Joubert Syndrome

Vincent Cantagrel,[1,17] Jennifer L. Silhavy,[1,17] Stephanie L. Bielas,[1] Dominika Swistun,[1] Sarah E. Marsh,[1] Julien Y. Bertrand,[2] Sophie Audollent,[3] Tania Attié-Bitach,[3] Kenton R. Holden,[4,5] William B. Dobyns,[6] David Traver,[2] Lihadh Al-Gazali,[7] Bassam R. Ali,[8] Tom H. Lindner,[9] Tamara Caspary,[10] Edgar A. Otto,[11] Friedhelm Hildebrandt,[11] Ian A. Glass,[12] Clare V. Logan,[13] Colin A. Johnson,[13] Christopher Bennett,[14] Francesco Brancati,[15] The International Joubert Syndrome Related Disorders (JSRD) Study Group,[18] Enza Maria Valente,[15] C. Geoffrey Woods,[16] and Joseph G. Gleeson[1,*]

Joubert syndrome (JS) and related disorders are a group of autosomal-recessive conditions sharing the "molar tooth sign" on axial brain MRI, together with cerebellar vermis hypoplasia, ataxia, and psychomotor delay. JS is suggested to be a disorder of cilia function and is part of a spectrum of disorders involving retinal, renal, digital, oral, hepatic, and cerebral organs. We identified mutations in *ARL13B* in two families with the classical form of JS. *ARL13B* belongs to the Ras GTPase family, and in other species is required for ciliogenesis, body axis formation, and renal function. The encoded Arl13b protein was expressed in developing murine cerebellum and localized to the cilia in primary neurons. Overexpression of human wild-type but not patient mutant *ARL13B* rescued the *Arl13b scorpion* zebrafish mutant. Thus, *ARL13B* has an evolutionarily conserved role mediating cilia function in multiple organs.

Introduction

Joubert syndrome (JS [MIM 213300]) is characterized by congenital cerebellar ataxia, hypotonia, oculomotor apraxia, and mental retardation. It is the most common inherited cerebellar malformation syndrome and is part of the autosomal-recessive cerebellar ataxia group of disorders.[1] The neuroradiological hallmark in JS is a peculiar malformation of the midbrain-hindbrain junction known as the "molar tooth sign" (MTS), consisting of cerebellar vermis hypoplasia or dysplasia, thick and horizontally oriented superior cerebellar peduncles, and an abnormally deep interpeduncular fossa.[2] The MTS has subsequently been reported in a group of syndromes termed Joubert syndrome and related disorders (JSRD). These include (1) classical JS (MIM 213300), (2) JS plus Leber congenital amaurosis (LCA, i.e., congenital retinal blindness [MIM 204000]),[3] (3) JS plus nephronophthisis (NPHP [MIM 256700]), (4) JS plus LCA plus NPHP (also known as cerebello-oculo-renal syndrome [CORS (MIM 608091)]),[4] (5) cerebellar vermis hypo/aplasia, oligophrenia, congenital ataxia, ocular coloboma, hepatic fibrosis (COACH [MIM 216360]) syndrome,[5] and (6) oral-facial-digital syndrome type VI[6,7] (MIM 277170), with occurrence of other features such as encephalocele and polydactyly variably found within each subgroup. Many of these disorders have previously been linked to genes encoding cilia-localized proteins, so JSRD was considered a candidate ciliopathy disorder. The recent discoveries that JSRD can be due to mutations in *CEP290*[8,9] (encoding a known centrosomal/cilia protein), as well as mutations in *NPHP1*[10,11] (previously implicated in the NPHP ciliopathy), *RPGRIP1L*[12–14] (encoding a binding partner of proteins implicated in the ciliopathy retinitis pigmentosa), and *TMEM67* (a.k.a. *MKS3*)[15] (previously implicated in the Meckel syndrome ciliopathy) have further strengthened the hypothesis that JSRD is due to defective ciliary function.

Here we report the identification of the JBTS8 locus and mutations in the *ARL13B* gene, encoding ADP-ribosylation factor-like protein 13B. ARL13B is a small GTPase belonging to the class of Arf/Arl family within the Ras superfamily of small GTPases involved in diverse cellular functions.

[1]Laboratory of Neurogenetics, Howard Hughes Medical Institute, Department of Neurosciences, University of California, San Diego, 9500 Gilman Drive, La Jolla, CA 92093-0691, USA; [2]Section of Cell and Developmental Biology, Division of Biological Sciences, University of California, San Diego, 9500 Gilman Drive, La Jolla, CA 92093-0380, USA; [3]Département de Génétique et INSERM U781, Hôpital Necker-Enfants Malades, 149 rue de Sèvres, 75743 Paris Cedex 15, France; [4]Neurosciences Section, Greenwood Genetic Center, 101 Gregor Mendel Circle, Greenwood, SC 29646, USA; [5]Departments of Neuroscience and Pediatrics, Medical University of South Carolina, Charleston, SC 29425, USA; [6]Department of Human Genetics, The University of Chicago, Room 319 CLSC, 920 E. 58th Street, IL 60637, USA; [7]Department of Pediatrics, [8]Department of Pathology, United Arab Emirates University, Faculty of Medicine and Health Sciences, PO Box 17666, Al-Ain, United Arab Emirates; [9]Division of Nephrology, Department of Internal Medicine III, University Clinic Leipzig, Philipp-Rosenthal-Str. 27, 04103 Leipzig, Germany; [10]Department of Human Genetics, Emory University School of Medicine, 615 Michael St. Suite 301, Atlanta, GA 30322-1047, USA; [11]Department of Pediatrics, University of Michigan, 8220C MSRB III, 1150 West Medical Center Drive, Ann Arbor, MI 48109-5640, USA; [12]Department of Pediatrics and Medicine, University of Washington School of Medicine, Childrens Hospital Regional Medical Center, A-7937, 4800 Sand Point Way NE, Seattle, WA 98105, USA; [13]Section of Ophthalmology and Neurosciences, Wellcome Trust Brenner Building, Leeds Institute of Molecular Medicine, [14]Yorkshire Regional Genetics Service, St James's University Hospital, Beckett Street, Leeds LS9 7TF, UK; [15]Instituto di Ricovero e Cura a Carattere Scientifico, Casa Sollievo della Sofferenza, Mendel Institute, viale Regina Margherita 261, 00198 Rome, Italy; [16]Department of Medical Genetics, Cambridge Institute for Medical Research, Wellcome/MRC Building, Addenbrooke's Hospital, Cambridge CB2 0XY, UK
[17]These authors contributed equally to this work
[18]Study group members are listed fully in the Supplemental Data
*Correspondence: jogleeson@ucsd.edu
DOI 10.1016/j.ajhg.2008.06.023.

ARL13B is thus the first gene encoding an enzymatically active protein implicated in JS, suggesting that its study may shed light on the essential signaling pathways. Furthermore, an *Arl13b* null mutation was recently identified as underlying the lethal *hennin* mouse mutant that displays a Sonic Hedgehog-like phenotype, as well as being identified in the zebrafish *scorpion* mutant that displays renal cysts and curved tail, both tied to impaired cilia function. The identification of *ARL13B* mutations in humans with JS, together with the previous work in mouse and zebrafish, indicates an extremely broad spectrum of phenotypes across species all related to defective cilia function. The results also suggest a role for cilia-mediated Sonic Hedgehog signaling in cerebellar development and the pathogenesis of JS in humans.

Material and Methods

Genome Mapping

Family MTI-001 was recruited according to an approved Human Subjects Protocol at the University of Leeds and UCSD. DNA was extracted from peripheral blood leukocytes by salt extraction, genotyped with the Illumina Linkage IVb mapping panel,[16] and analyzed with easyLINKAGE-Plus[17] software, which runs Allegro version 1.2c in a PC Windows interface to calculate multipoint LOD scores. Parameters were set to autosomal recessive with full penetrance, and disease allele frequency of 0.001. Genomic regions with LOD scores over 2 were considered as candidate intervals. Linkage simulations were performed with Allegro 1.2c under the same parameters, with 500 markers at average 0.64 cM intervals, codominant allele frequencies, and parametric calculations.[17] Additional subjects were enrolled according to approved protocols at University of Chicago, University of Michigan, University of Leeds, and Necker Hospital in Paris. Control samples were from healthy US adult subjects from a hypertension study, from healthy Arab controls from the United Arab Emirates, and healthy Pakistani controls from Leeds, UK.

Mutation Screening

We performed direct bidirectional sequencing of the ten coding exons and splice junction sites of *ARL13B* via BigDye Terminator cycle sequencing (Applied Biosystems). We screened 124 patients ascertained for the presence of nephronophthisis with or without features of Joubert syndrome (courtesy of Friedhelm Hildebrandt, U. Michigan) and 32 patients ascertained for the presence of Meckel syndrome with or without features of Joubert syndrome (courtesy of Tania Attie-Bitach, Necker Hospital, France) via bidirectional sequencing. We screened 44 patients ascertained for the presence of Meckel syndrome with or without features of Joubert syndrome (courtesy of Colin Johnson, U. Leeds) by LightScanner detection (Idaho Technologies), with subsequent bidirectional sequencing of aberrant bands. All patient samples were ascertained and managed according to approved human subjects protocols.

Candidate Genes and GenBank Accession Numbers

Human *ARL6* has two GenBank numbers (NM_032146.1 and NM_177976.3) encoding the same protein, but the first encodes a longer transcript. Human *ARL13B* has two GenBank numbers (NM_144996.1 and NM_144996.2) differing in that the second entry is missing coding exons 2–3. Zebrafish *arl13B* has GenBank number NM_173272. Mouse *Arl13b* has GenBank number NM_026577.2.

Bioinformatics

Predicted folding and intermolecular interactions were predicted with Swiss-Model with crystallized ARL2-GTP as a template. The resulting ARL13B structure was manipulated and rendered with PyMOL software by importing amino acid sequence for wild-type and mutant and comparing the predicted hydrogen bonds.

GTP Binding Assay

Human wild-type and mutant *ARL13B* cDNA were cloned separately into the pGEX 6P1 vector (GE Lifesciences), and GST-tagged purified protein was isolated according to the manufacturer's recommendations. Protein was retrieved from the soluble phase, integrity verified by SDS-PAGE analysis followed by Coomassie staining, and analyzed by circular dichroism to validate that wild-type and mutant proteins had similar secondary structure as described. GTP binding was performed with a filter-based assay as described,[18] with denatured (boiled for 15 min) Arl13b protein as negative control and Rac as a positive control, and analyzed with SigmaPlot Ver 10.0, with one-way ANOVA for statistical analysis.

Zebrafish Characterization

The *arl13b*$^{sco/+}$ line was obtained from the Zebrafish International Resource Center (ZIRC) under an approved animal protocol at UCSD. One-cell embryos from *arl13b*$^{sco/+}$ matings were injected with 50 pg in vitro transcribed capped open reading frame RNA (Ambion Message Kit) of human wild-type or mutant transcript. After 72 hr, embryos were phenotyped by an investigator that was blinded to the genotype, and then all embryos were subject to genotyping for correlation.

Histology

Mouse tissue was fixed with 4% paraformaldehyde, then processed for 15 μm cryostat sections and immunostained as described.[19] We used two different rabbit polyclonal antibodies for Arl13b, one that was recently created against a bacterially expressed GST fused to amino acids 208–428 of murine Arl13B,[19] and one created against an internal polypeptide, which behaved similarly, so only the first was used for further experimentation. Neither antibody showed reactivity with the cilia in the *hennin* mutant[19] (data not shown). Antibodies were used at the following concentrations: Arl13b, 1:2000; acetylated tubulin (Zymed 32-2700), 1:500; calbindin (Swant), 1:600. Cerebellar granule neurons were isolated with a cell-density gradient as described,[20,21] fixed, and immunostained at various time points after plating.

Results

Identification of the JBTS8 Locus at the Centromeric Region of Chromosome 3

In our series, we excluded linkage to known loci in 27 consanguineous JSRD families, supporting evidence for further genetic heterogeneity. One of the largest families (MTI-001, Figure 1A), which is of Pakistani origin and the first to be recruited in this study, displayed a proven MTS on brain imaging (Table S1 available online), provided a maximum expected LOD score of 3.0, and did not display any mutations

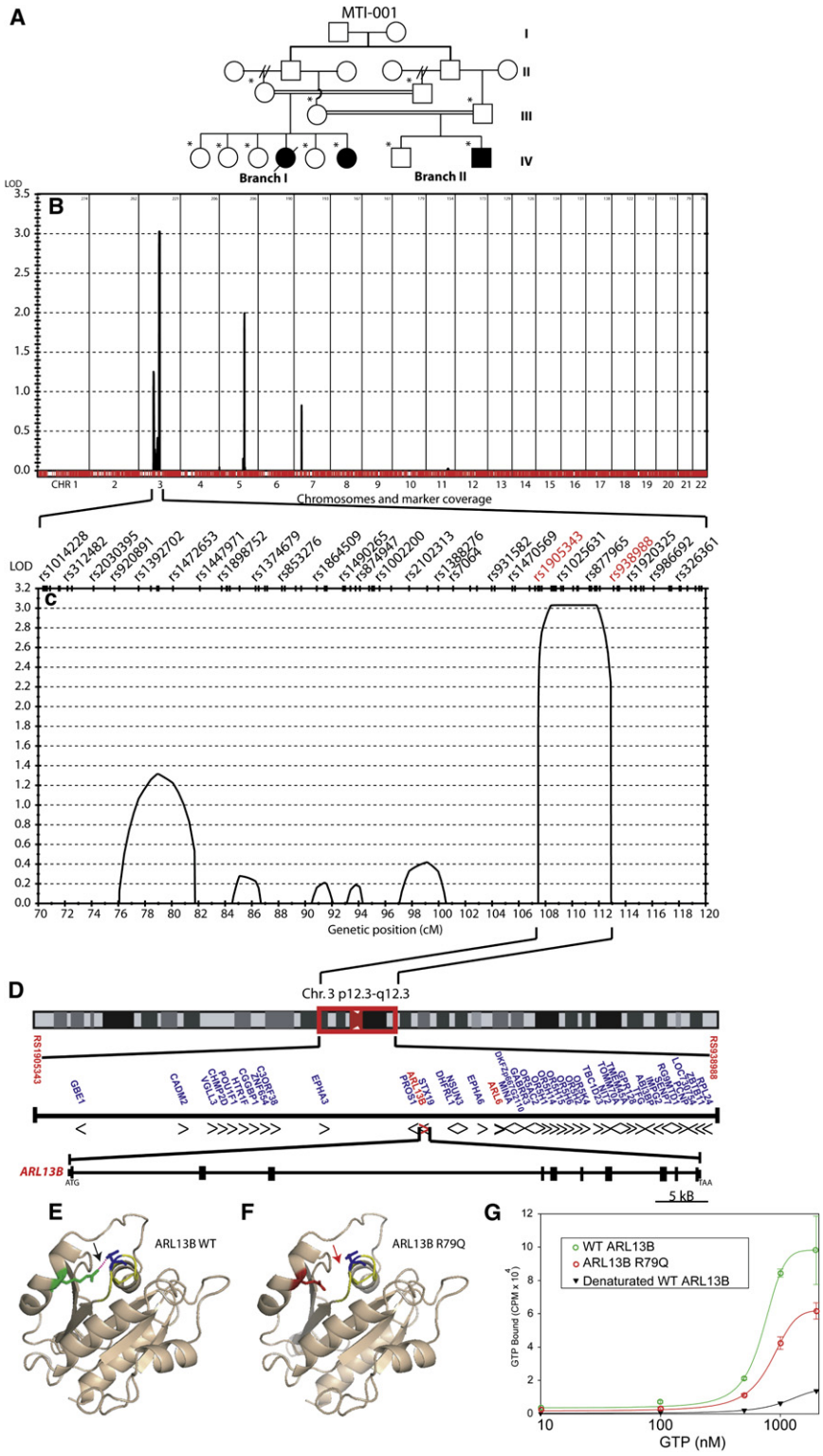

Figure 1. Mapping JSRD Family MTI-001 Identified the JBTS8 Locus Containing the *ARL13B* Gene, Mutation of which Produces Altered GTP Binding

(A) MTI-001 consists of a double first cousin marriage where each of two brothers were married twice (generation II, double hash refers to divorce); one had two half-brothers and one had two half-sisters, and each of those subsequently married his/her respective cousin (generation III). These two couples each produced an affected offspring (filled symbols in generation IV) as well as healthy siblings. One affected girl from branch 1 died from related medical complications (single hash line).

(B) Whole-genome analysis of linkage results with chromosomal position (*x* axis) and multipoint LOD scores (*y* axis) showing a significant LOD score (>3) on chr. 3. No other peaks reached this threshold for significance.

(C) Expanded view of the candidate interval showing that the linkage signal is composed of one major peak defined by recombinations at rs1005343 and rs938988 SNP markers (red), thus defining a minimal candidate interval from 107 to 112 cM.

(D) Expanded view of the candidate interval on chr. 3p12.3-q12.3, encompassing the centromere, containing 41 candidate genes, including *ARL6* and *ARL13B* (red). Transcriptional direction indicated by arrowheads. Genomic structure of *ARL13B* consists of 10 coding exons extending over about 70 KB of genomic sequence.

(E) Homology modeling of wild-type ARL13B showing R (green) residue and predicted hydrogen bond (red dashed line) with D (blue) residue that engages in GTP binding.

(F) The p.R79Q mutation is a basic polar to neutral polar substitution (red) and is predicted to disrupt this hydrogen bond (absent dashes indicated by red arrow).

(G) GTP binding assay via recombinant wild-type ARL13B (green) or p.R79Q mutant (red) showing altered kinetics and binding capacity. Experiment performed in triplicate. Error bars represent SEM. Negative control was denatured wild-type ARL13B (black). Statistical differences observed between wild-type and mutant at 500, 1000, and 2000 nM GTP concentration (*$p < 0.05$, one-way ANOVA).

in any of the five known JSRD genes (*NPHP1, AHI1, CEP290, MKS3, RPGRIP1L*). We performed a 0.64 cM resolution genome-wide screen by the Illumina Whole Genome SNP Linkage IVb panel, which defined an interval of 107–112 cM (80.0–103.3 MB) on chromosome 3p12.3-q12.3, with peak multipoint LOD score of 3.0 termed JBTS8 (Figure 1B).

Patients from MTI-001 Have a Homozygous p.R79Q Change in the *ARL13B* Gene

This interval encompassed the centromere, with 41 genes, and markers rs1905343 and rs938988 formed the p- and q-arm breakpoints, respectively (Figure 1C). Four genes within this interval were listed within the cilia proteome

databases,[22,23] based upon the original work that identified these proteins as localized to or predicted to function at the cilium,[24–30] including *CEP97*, *MINA*, *ARL6*, and *ARL13B*, and thus were considered as strong candidates (Figure 1D). Of these, only *ARL6* (ADP-ribosylation factor-like 6) had been implicated in a human disease, where mutations are the cause of Bardet-Biedl syndrome 3 (BBS3).[31,32] Because predominantly missense mutations were identified in *ARL6*, and because JSRD is a phenotypically more severe disorder than BBS, we considered that more severe mutations (such as stop codon or splice site mutations) might be found in MTI-001. Therefore, the seven coding exons of *ARL6* were sequenced in affecteds from this family, but no sequence changes were encountered. The *ARL13B* gene (also known as *ARL2L1*, or *Y37E3.5* in *C. elegans*) had previously been demonstrated to be expressed in ciliated neurons and specifically found to localize to the ciliary axoneme in *C. elegans* sensory neurons,[25,31] so we considered this the next-most-likely candidate gene. Sequence analysis identified a homozygous c.G236A mutation in exon 3 that is predicted to lead to a p.R79Q (positively charged to noncharged) amino acid substitution (Figure S1). This mutation was not encountered in 288 individuals (96 of Pakistani origin, 96 individuals of Arab origin, 96 of mixed US origin), providing >80% power to distinguish this from a normal sequence variant,[33] and suggesting that it does not represent a common allele. Genotyping of all members of MTI-001 showed that this homozygous mutation segregated with the phenotype in affecteds but not in unaffecteds or obligate carriers.

Impaired GTP Binding Associated with the R79Q Mutation

The p.R79Q mutation identified in family MTI-001 occurred within the highly conserved GTP-binding domain.[34,35] Therefore, we questioned whether this mutation might affect GTP binding. Because ARL13B is 36% identical and 61% similar in amino acid sequence with ARL2, we used the crystal structure of ARL2 to model the effect of the p.R79Q mutation on intramolecular forces. This modeling showed that R79 (R74 in ARL2) of the switch II domain establishes a hydrogen bond with D30 (D25 in ARL2) of the P loop domain. This interaction is conserved in other ARF family proteins[36] and is predicted to be disrupted with alteration in amino acid charge because of the p.R79Q substitution (Figures 1E and 1F), and as a result might disrupt GTP binding. To test this hypothesis, we cloned both wild-type and p.R79Q ARL13B human cDNAs into bacterial expression vectors (Figure S2), isolated recombinant proteins (Figure S3), verified that both were soluble based upon their isolation from the liquid phase and that they had similar secondary structure based upon similar circular dichroism analysis[37] (not shown), and then tested their ability to bind GTP in an established in vitro binding assay. We found that the concentration for half-maximal GTP binding by ARL13B was ~7.2×10^{-7} M. At this concentration, the amount of GTP bound to the mutant protein was about half of the amount bound to the wild-type protein ($p < 0.05$ for each of three comparisons), whereas negative control was just above background (Figure 1G). We conclude that the p.R79Q mutation interferes with GTPase binding activity of ARL13B and that this mutation could lead to impairment of its cilia function.

Mutation Analysis in a JS Cohort

We tested for mutations in *ARL13B* within several cohorts of JSRD. By using bidirectional sequencing, we screened 182 patients from our cohort diagnosed with JSRD and identified two additional mutations in one family. Family MTI-423 has one affected female displaying a proven MTS on brain imaging (Figure S4). The affected female displayed a compound heterozygous mutation c.G246A (exon 3) resulting from a stop codon p.W82X from the mother and a c.C598T (exon 5) from the father that results in a positive charged to uncharged amino acid p.R200C missense mutation within the coiled-coil domain (Figure 2A; Figure S1). This family did not display mutations in any of the known JSRD genes (*NPHP1*, *AHI1*, *CEP290*, *TMEM67*, *RPGRIP1L*). Each of these *ARL13B* substitution mutations was fully conserved across evolution in all mammals as well as *Xenopus tropicalis*, *Danio rerio*, and *Tetraodon Nigroviridis* (Figure 2B), and none of these mutations or any other predicted functional changes were identified by direct bidirectional sequencing of genomic DNA in a cohort of 182 healthy individuals (364 chromosomes). The early lethality of the *hennin* mouse suggests a critical role for *ARL13B* in early embryonic development and may provide one explanation for the low percentage of *ARL13B* mutations in the JSRD cohort and the low representation of truncating mutations among the *ARL13B* patients.

Delineation of the Phenotypic Spectrum Associated with ARL13B Mutations

The phenotype observed in patients with identified mutations consists predominantly of classical Joubert syndrome. All patients displayed the MTS (Table S1). In MTI-001, two affecteds each displayed a small occipital encephalocele. In the other family, there was no occipital encephalocele, and there were no other supratentorial cerebral abnormalities and no renal abnormalities upon diagnostic ultrasound (performed on both families). Study of urinary concentration defects may be a more sensitive measure of early kidney involvement and was not available on any of these patients, so it is possible that renal symptoms might develop in the future. One affected from MTI-001 (now deceased) displayed evidence of mild nonspecific pigmentary retinopathy on clinical examination, although electroretinogram was normal on the affected siblings, so the involvement of *ARL13B* in retinal function is not yet clear. We also screened a cohort of 124 patients with JS with nephronophthisis and a cohort of 76 patients with overlapping Meckel syndrome with JS features. No

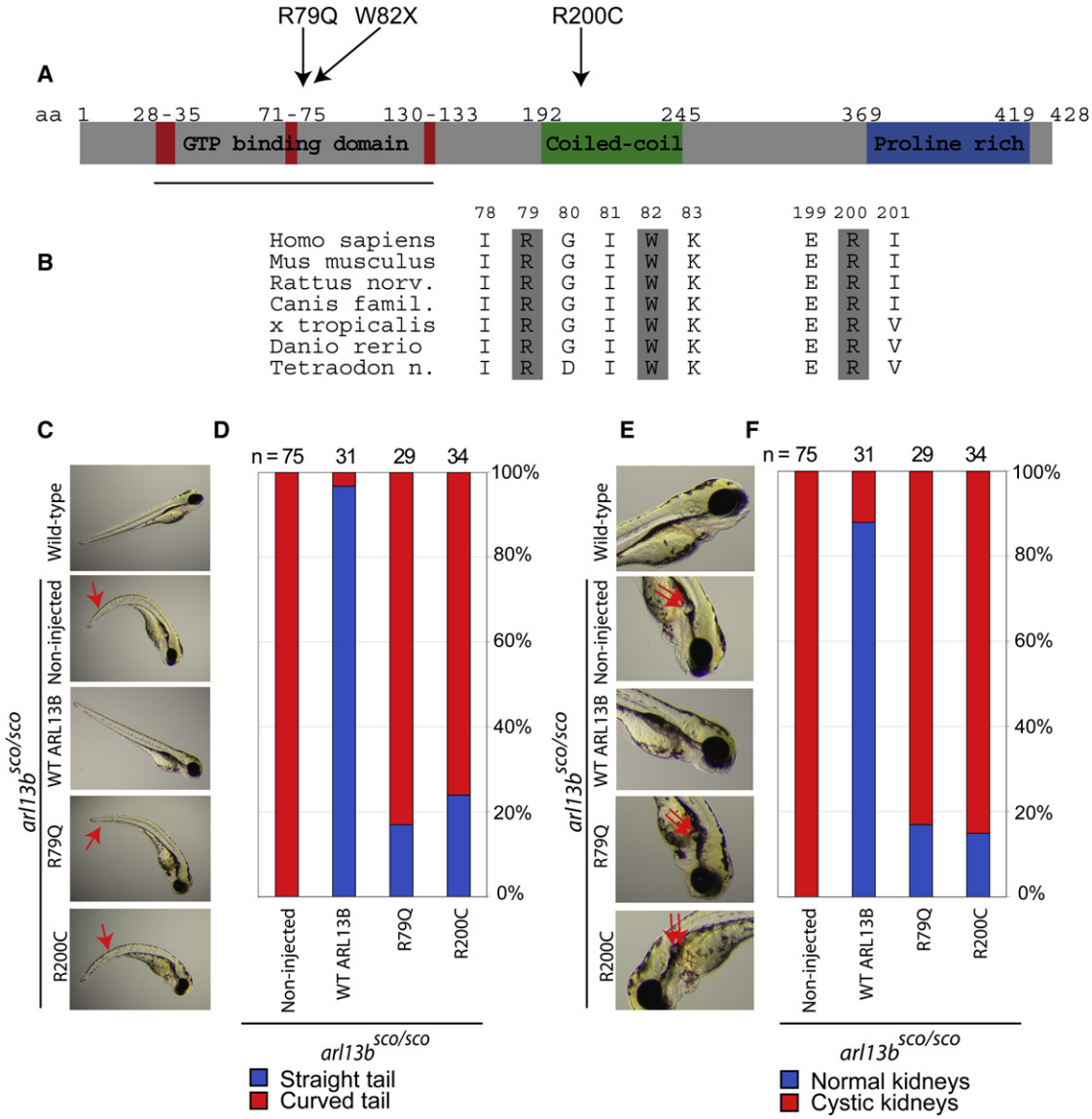

Figure 2. Human Mutations in ARL13B Occur in Conserved Residues and Interfere with Evolutionarily Conserved Functions
(A) Domain structure of ARL13B protein, with GTP binding, coiled-coil, and proline-rich domains. Red indicates conserved regions involved in GTP binding. Mutations are indicated along the top.
(B) Evolutionary conservation of ARL13B, showing that each mutated residues is conserved at least to *Danio rerio* (zebrafish).
(C–F) Wild-type zebrafish have straight tails and absence of cystic kidney. Noninjected *arl13b*$^{sco/sco}$ embryos have curved tails (red arrow) and cystic kidneys (double red arrow). The *arl13b*$^{sco/sco}$ embryos injected with human wild-type *ARL13B* RNA show rescue of the curved tail and absence of cystic kidney. The human p.R79Q and p.R200C mutant *ARL13B* RNA failed to rescue either phenotype in the majority of embryos, although about 15%–24% showed evidence of rescued phenotype, suggesting a hypomorphic allele. A control amino acid substitution (p.S371I) in *ARL13B* showed a rescue effect similar to wild-type (not shown).

mutation in either of these cohorts was encountered, suggesting that mutations in *ARL13B* are restricted to the classical form of JSRD (which can include encephalocele and retinopathy)[38] and are not identifiable in other related ciliopathies, at least at this level of detection.

Human Wild-Type but Not Mutated ARL13B Rescue the Zebrafish Scorpion Mutant

To test the evolutionary conservation of *ARL13B*, we utilized zebrafish (*Danio rerio*). Comparison of the human and zebrafish *ARL13B* shows 75% similarity and 59% identity in more than 90% of the predicted amino acid sequence. We took advantage of the *scorpion* zebrafish mutant in the *arl13b* locus.[39] The *arl13b*^{sco} allele is due to a retroviral insertion into the first exon, which inactivates the gene, as evidenced by the finding that morpholino antisense treatment against *arl13b* produced a phenocopy of the *arl13b*$^{sco/sco}$ mutant.[40] These mutants display fully penetrant curved tail and cystic kidney phenotypes, which are evident by 72 hr post fertilization (hpf) (n = 75, Figures

2C and 2E). We tested for rescue of the phenotype upon injection of RNA into 1-cell stage embryos from *arl13b*$^{sco/+}$ × *arl13b*$^{sco/+}$ matings, which produce 1/4 *arl13b*$^{sco/sco}$ embryos, by phenotyping the fish at 72 hpf by investigators blinded to the genotype. Injection of RNA corresponding to the zebrafish *arl13b* cDNA caused complete rescue of the phenotype, as evidenced by the fact that no mutants were identified by this blinded genotyping protocol (n = 20). Injection of the human *ARL13B* RNA similarly rescued the phenotype in the majority of embryos (Figures 2D and 2F). Among these mutants, the curved tail phenotype was rescued in 97% and the cystic kidney was rescued in 88% of embryos (n = 31). There was no overt overexpression phenotype that resulted from injection of either RNA into wild-type sibling embryos. Thus, the *ARL13B* gene displays evolutionarily conserved functions at the genetic level in embryogenesis.

In order to test the functional impairment of the patient missense mutations, we injected RNA corresponding to the cDNA for the human open reading frame of *ARL13B*, with each of these mutations introduced into the coding region in a similar assay. We opted to use the human rather than the zebrafish cDNA for this work, because it represented a more stringent test of function of the human mutations. Injection of each of these mutant RNAs resulted in a marked reduction in rescue when compared with the wild-type human RNA or a control nonpathogenic amino acid substitution-containing RNA. For this control, we chose the p.S371I transversion, because S371 is an evolutionarily conserved amino acid (similar to R79 and R200), it occurs in a part of the protein without known secondary structure, and the p.S371I alteration does not change the charge of the residue. The curved tail phenotype was rescued in 17% and 24%, and the cystic kidney phenotype was rescued in 17% and 15% of the *arl13b*$^{sco/sco}$ mutants for the p.R79Q and p.R200C mutations, respectively (n = 29 for p.R79Q, 34 for p.R200C, Figures 2C–2F). Contrarily, for the p.S371I control substitution, the curved tail phenotype was rescued in 100% and the cystic kidney phenotype was rescued in 91% of the *arl13b*$^{sco/sco}$ mutants (n = 11 for p.S371I, not shown). These data indicate that the human RNA with these human pathogenic mutations fail to function as well as the wild-type or control mutagenized human RNA and suggests that these pathogenic mutations at least partially impair the function of the protein during embryogenesis, leading to the JSRD phenotype.

Arl13b Is Expressed in Organs Affected in JS, with Protein Localized to Cilia

We next tested for expression of Arl13b in mouse tissues that are involved in JSRD patients at the presumed time points of affection to determine whether expression of the protein might account for the human phenotype. Arl13b protein was localized to cilia of all organs examined where they are known to be present, including the developing cerebellum (Figure 3). The epithelial cells lining the distal renal collecting ducts have well-described cilia, and we observed Arl13b staining of cilia structures within these tubules (Figure 3A). This staining might predict a role for Arl13b in kidney function, although none of our patients with *ARL13B* mutations displayed evidence of impaired kidney function. The retinal photoreceptor inner and outer segments, corresponding to the cell body and rhodopsin-containing disks, are bridged by a connecting cilium. We observed robust Arl13b staining of the connecting cilium at P10 (Figure 3B), similar to many of the proteins involved in LCA.[41,42] It is interesting to note that one of the patients with an *ARL13B* mutation displayed evidence of retinopathy (Table S1). It will be important to follow the remaining patients to determine whether they develop progressive involvement of these organs in the future.

To test for expression in the developing cerebellum, the major site of involvement in JSRD, we examined Arl13b localization in postnatal mice. At the P0 time point, the cerebellum displays well-developed folia and consists of three well-defined layers: the external granule layer (EGL), Purkinje cell layer (PCL), and internal granule layer (IGL). Granule neuron precursors proliferate and migrate parallel to the surface of the cerebellum within the EGL. Postmitotic granule neurons then migrate radially into the cerebellar parenchyma and past the PCL to settle in the IGL. We detected strong staining of cilia-like structures on granule neurons both in the EGL and IGL (Figure 3C), which is consistent with previous serial electron microscopic sectioning of the cerebellum,[43,44] as well as recent studies that have used staining for adenylate cyclase III to label cilia.[45,46] Staining of Arl13b across the spectrum of cerebellar development in mouse demonstrated cilia-like structures in granule neuron populations, both in the EGL and IGL (Figure S5). There was a time dependence to the staining of cilia-like structures during cerebellar development, with about 40% of cells showing an immunopositive cilia at E16, dropping to less than 1% of cells by P21.

In order to be certain that these ARL13B-immunopositive structures represented cilia, we obtained sections from the cerebellum at P0 in a transgenic mouse that expresses EGFP fused to Centrin 2, a constitutive centrosome/basal body marker that localizes to centrioles.[47] As expected, we found that most cells in the EGL contained a readily identifiable pair of centrioles adjacent to the nucleus, representing the basal body. We found an immunopositive ARL13B structure emanating from the region surrounding the basal body in many of these cells (Figure 3C), thereby demonstrating the spatial relationship between the two structures and suggesting that ARL13B marks the cilium. However, in many cells, ARL13B was not identified near a pair of centrioles, suggesting the possibility that ARL13B stains the cilia in only a fraction of granule neurons or that only a fraction of granule neurons contain a cilium.

In order to differentiate between these possibilities, we isolated cerebellar granule neuron precursors from P5 mouse by using a cell-density gradient, cultured and fixed

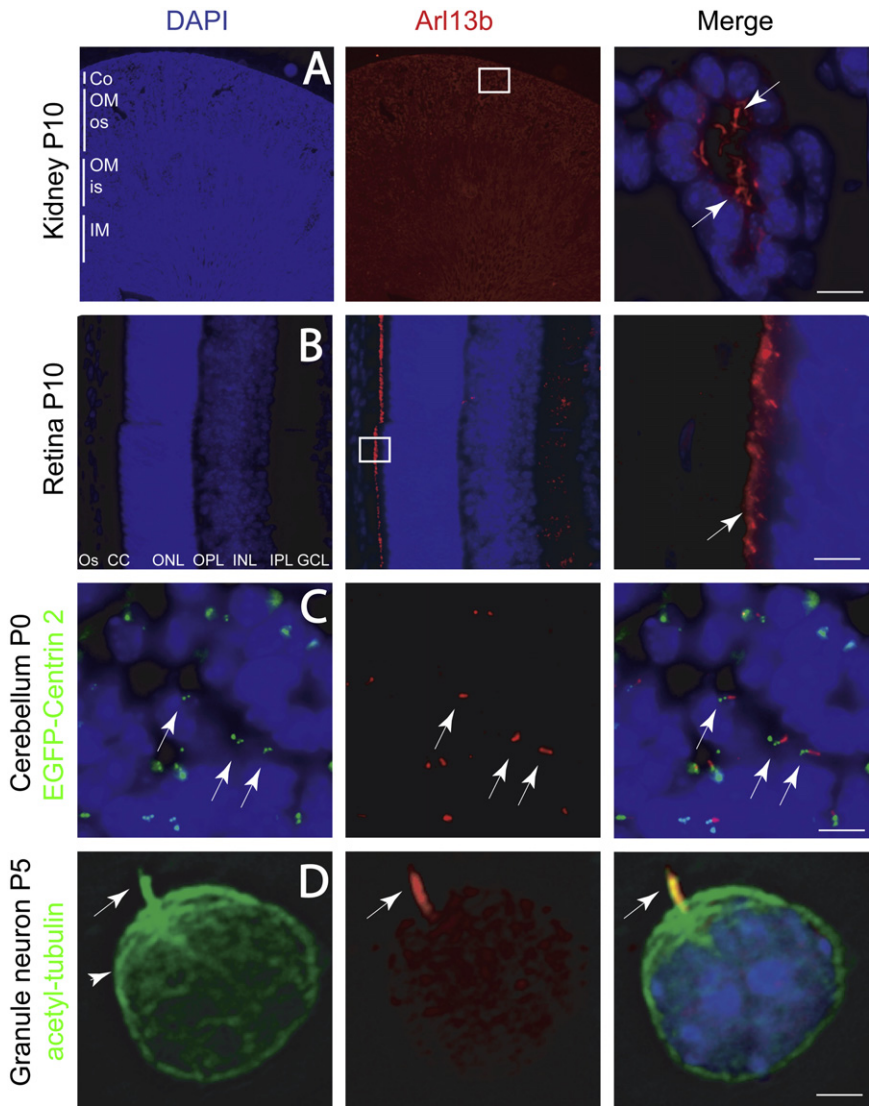

Figure 3. Arl13b Localization in Cilia within Kidney, Retina, and Developing Cerebellar Granule Neurons

Boxed region indicates location of high-power field shown in the third panel in (A) and (B).

(A) Kidney tubule shows Arl13b-positive cilia protruding into the lumen (arrows) in close approximation to the epithelial nuclei (blue, DAPI).

(B) Retina shows intense Arl13b staining in photoreceptor connecting cilia layer (CC, arrow).

(C) External granule layer (EGL) of P0 cerebellum from EGFP-Centrin 2 transgenic mouse stained with Arl13b. EGFP-labeled centrioles (green dots, arrow, left) are evident in many cells, defining the position of the basal body. An Arl13b-positive cilium projects adjacent to the basal body in many of these cells (arrows, right).

(D) Acutely dissociated CGN showing cilia (arrow) stained with acetylated tubulin (green) costains with Arl13b (red). Acetylated tubulin also stains the microtubule cytoskeleton (arrowhead), which is negative for Arl13b.

Abbreviations: Co, cortex; os, outer stripe of medulla; is, inner stripe of medulla; OM, outer medulla; IM, inner medulla; GCL, ganglion cell layer; IPL, inner plexiform layer; INL, inner nuclear layer; OPL, outer plexiform layer; ONL, outer nuclear layer; CC, connecting cilia; OS, outer segment; P, postnatal day. Scale bar represents 20 μm in (A)–(C) and 5 μm in (D).

at various time points. We found that a fraction of these primary cultured neurons display a cilia, as evidenced by labeling of a structure protruding from the cell body that was positive for acetylated tubulin (Figure 3D). Although the acetylated tubulin staining was strongly positive in the cilia, it extended into many of the microtubules within the cell soma. All cells with a cilium based upon this staining also displayed immunopositivity for Arl13b, and Arl13b staining was largely restricted to the cilia. Thus, Arl13b appears to be a sensitive and specific marker for the cilium in many cells including in the developing cerebellum. The data also support a role for Arl13b in the pathogenesis of JSRD, and thus strongly links JSRD to other human ciliopathies.

Discussion

ARL13B encodes ADP-ribosylation factor-like protein 13B (previously known as ADP-ribosylation factor-like protein 2-like 1) and belongs to the small Ras GTPase superfamily. ADP-ribosylation factor (ARF) GTP-binding proteins are among the best-characterized members of the Ras superfamily of GTPases, with well-established roles in membrane trafficking pathways. However, the ARL proteins appear to be functionally distinct, and many have roles in microtubule function.[48,49] A mutation in *Arl13b* was very recently identified as the cause for the murine *hennin* phenotype that displays a disrupted neural tube during embryogenesis.[19] The encoded Arl13b protein is localized to the primary cilia where it presumably plays a role in microtubule assembly or transport akin to the roles of other Arl proteins. However, the *Arl13b*$^{hnn/hnn}$ mutant is lethal at embryonic day 13.5–14.5 because of the severe cilia phenotype, thereby precluding a more detailed analysis of later functions.

Currently, mutations are identified in *CEP290* in about 40% of patients that also display NPHP and LCA,[50] in *AHI1* in 10%–20% of patients mostly without NPHP,[51,52] and in probably lower percentages in *TMEM67*, *NPHP1*, and *RPGRIP1L* genes. Although there are two additional

JS loci (JBTS) that have been described where the causative gene has not yet been reported,[53–55] fewer than 10% of families map to these loci.[56] Thus, fewer than 50% of patients can receive a molecular diagnosis, and genotype-phenotype correlations subsequently are not yet clarified. Our preliminary data indicate that mutations in *ARL13B* are identified probably in less than 1% of JS, akin to the mutation frequency of *ARL6* in BBS, although it will be interesting to determine the frequency of mutations in *ARL13B* among larger cohorts of JSRD patients.

Akin to the findings in BBS3, which is the only other disease to be linked to mutations in an ARL protein, the majority of mutations identified in *ARL13B* to date are missense.[31,32] Additionally, our zebrafish data indicate that the missense mutations are probably hypomorphic alleles, because expression of each missense mutation rescues the phenotype with intermediate potency in the *arl13b*$^{sco/sco}$ mutant. This most likely reflects a requirement for the protein during embryogenesis, because both *Arl3* and *Arl13b* mutant mice are often lethal prior to birth.[19,57] Because *Arl13b* has been implicated in Sonic hedgehog (Shh) signaling,[19] and because Shh[58,59] as well as genes critical in cilia function have been implicated in proliferation of cerebellar granule neuron precursors,[46,60] our data suggest that Joubert syndrome may represent a defect in cilia function mediating Shh signaling in this proliferation, although the exact signaling mechanisms and disrupted developmental pathways remain to be discovered.

Supplemental Data

Supplemental Data include a list of other members of the International JSRD Study Group, five figures, and one table and are available at http://www.ajhg.org/.

Acknowledgments

We thank the Marshfield Clinic Research Foundation and the US National Heart, Lung, and Blood Institute for genotyping support; the UCSD Neurosciences Microscopy Core for imaging (P30 NS047101); Jeong-Soo Lee (Dana Farber Cancer Institute) for the zebrafish *arl13b* clone; Mark Lawson (UCSD) for help with SigmaPlot and statistical analysis; Daniel O'Connor (UCSD) for control DNA samples; and members of the Gleeson laboratory for helpful discussions. Genotyping services were provided by the Center for Inherited Disease Research (CIDR). CIDR is fully funded through a federal contract from the National Institutes of Health to The Johns Hopkins University, contract number N01-HG-65403. F.H. is supported by NIH grants R01-DK068306, R01-DK064614, and R01-DK069272 and is a Doris Duke Distinguished Clinical Scientist. V.C. was supported by a French Foundation for Medical Research (FRM) fellowship. S.L.B. was supported by the Neuroplasticity of Aging Postdoctoral Training Grant (T32 AG00216). J.Y.B. was supported by the Irvington Institute Fellowship Program of the Cancer Research Institute. This work was supported by grants from the US National Institute of Neurological Disease and Stroke, the Simons Foundation, and the Burroughs Wellcome Fund Award in Translational Research (to J.G.G.). The authors report no conflict of interest.

Received: May 12, 2008
Revised: June 11, 2008
Accepted: June 30, 2008
Published online: July 31, 2008

Web Resources

The URLs for data presented herein are as follows:

BLAST, http://www.ncbi.nlm.nih.gov/
Pfam database, http://www.sanger.ac.uk/Software/Pfam/
Human Genome Browser, http://www.genome.ucsc.edu/
Online Mendelian Inheritance in Man (OMIM), http://www.ncbi.nlm.nih.gov/Omim/
Cilia Proteome, http://www.ciliaproteome.org/ and http://www.bcgsc.ca/
Zebrafish database, http://zfin.org/
Zebrafish International Resource Center, http://zebrafish.org/zirc/home/guide.php/
Pymol, http://www.pymol.org
Swiss-Model, http://swissmodel.expasy.org/

References

1. Palau, F., and Espinos, C. (2006). Autosomal recessive cerebellar ataxias. Orphanet J. Rare Dis. *1*, 47.
2. Maria, B.L., Hoang, K.B., Tusa, R.J., Mancuso, A.A., Hamed, L.M., Quisling, R.G., Hove, M.T., Fennell, E.B., Booth-Jones, M., Ringdahl, D.M., et al. (1997). "Joubert syndrome" revisited: Key ocular motor signs with magnetic resonance imaging correlation. J. Child Neurol. *12*, 423–430.
3. King, M.D., Dudgeon, J., and Stephenson, J.B. (1984). Joubert's syndrome with retinal dysplasia: neonatal tachypnoea as the clue to a genetic brain-eye malformation. Arch. Dis. Child. *59*, 709–718.
4. Satran, D., Pierpont, M.E., and Dobyns, W.B. (1999). Cerebello-oculo-renal syndromes including Arima, Senior-Loken and COACH syndromes: more than just variants of Joubert syndrome. Am. J. Med. Genet. *86*, 459–469.
5. Verloes, A., and Lambotte, C. (1989). Further delineation of a syndrome of cerebellar vermis hypo/aplasia, oligophrenia, congenital ataxia, coloboma, and hepatic fibrosis. Am. J. Med. Genet. *32*, 227–232.
6. Haug, K., Khan, S., Fuchs, S., and Konig, R. (2000). OFD II, OFD VI, and Joubert syndrome manifestations in 2 sibs. Am. J. Med. Genet. *91*, 135–137.
7. Gleeson, J.G., Keeler, L.C., Parisi, M.A., Marsh, S.E., Chance, P.F., Glass, I.A., Graham, J.M. Jr., Maria, B.L., Barkovich, A.J., and Dobyns, W.B. (2004). Molar tooth sign of the midbrain-hindbrain junction: occurrence in multiple distinct syndromes. Am. J. Med. Genet. *125A*, 125–134.
8. Valente, E.M., Silhavy, J.L., Brancati, F., Barrano, G., Krishnaswami, S.R., Castori, M., Lancaster, M.A., Boltshauser, E., Boccone, L., Al-Gazali, L., et al. (2006). Mutations in CEP290, which encodes a centrosomal protein, cause pleiotropic forms of Joubert syndrome. Nat. Genet. *38*, 623–625.
9. Sayer, J.A., Otto, E.A., O'Toole, J.F., Nurnberg, G., Kennedy, M.A., Becker, C., Hennies, H.C., Helou, J., Attanasio, M., Fausett, B.V., et al. (2006). The centrosomal protein nephrocystin-6 is mutated in Joubert syndrome and activates transcription factor ATF4. Nat. Genet. *38*, 674–681.

10. Castori, M., Valente, E.M., Donati, M.A., Salvi, S., Fazzi, E., Procopio, E., Galluccio, T., Emma, F., Dallapiccola, B., and Bertini, E. (2005). NPHP1 gene deletion is a rare cause of Joubert syndrome related disorders. J. Med. Genet. *42*, e9.
11. Parisi, M.A., Bennett, C.L., Eckert, M.L., Dobyns, W.B., Gleeson, J.G., Shaw, D.W., McDonald, R., Eddy, A., Chance, P.F., and Glass, I.A. (2004). The NPHP1 gene deletion associated with juvenile nephronophthisis is present in a subset of individuals with Joubert syndrome. Am. J. Hum. Genet. *75*, 82–91.
12. Arts, H.H., Doherty, D., van Beersum, S.E., Parisi, M.A., Letteboer, S.J., Gorden, N.T., Peters, T.A., Marker, T., Voesenek, K., Kartono, A., et al. (2007). Mutations in the gene encoding the basal body protein RPGRIP1L, a nephrocystin-4 interactor, cause Joubert syndrome. Nat. Genet. *39*, 882–888.
13. Delous, M., Baala, L., Salomon, R., Laclef, C., Vierkotten, J., Tory, K., Golzio, C., Lacoste, T., Besse, L., Ozilou, C., et al. (2007). The ciliary gene RPGRIP1L is mutated in cerebello-oculo-renal syndrome (Joubert syndrome type B) and Meckel syndrome. Nat. Genet. *39*, 875–881.
14. Vierkotten, J., Dildrop, R., Peters, T., Wang, B., and Ruther, U. (2007). Ftm is a novel basal body protein of cilia involved in Shh signalling. Development *134*, 2569–2577.
15. Baala, L., Romano, S., Khaddour, R., Saunier, S., Smith, U.M., Audollent, S., Ozilou, C., Faivre, L., Laurent, N., Foliguet, B., et al. (2007). The Meckel-Gruber syndrome gene, MKS3, is mutated in Joubert syndrome. Am. J. Hum. Genet. *80*, 186–194.
16. Murray, S.S., Oliphant, A., Shen, R., McBride, C., Steeke, R.J., Shannon, S.G., Rubano, T., Kermani, B.G., Fan, J.B., Chee, M.S., et al. (2004). A highly informative SNP linkage panel for human genetic studies. Nat. Methods *1*, 113–117.
17. Hoffmann, K., and Lindner, T.H. (2005). easyLINKAGE-Plus—automated linkage analyses using large-scale SNP data. Bioinformatics *21*, 3565–3567.
18. Tisdale, E.J. (1999). A Rab2 mutant with impaired GTPase activity stimulates vesicle formation from pre-Golgi intermediates. Mol. Biol. Cell *10*, 1837–1849.
19. Caspary, T., Larkins, C.E., and Anderson, K.V. (2007). The graded response to Sonic Hedgehog depends on cilia architecture. Dev. Cell *12*, 767–778.
20. Tanaka, T., Serneo, F.F., Higgins, C., Gambello, M.J., Wynshaw-Boris, A., and Gleeson, J.G. (2004). Lis1 and doublecortin function with dynein to mediate coupling of the nucleus to the centrosome in neuronal migration. J. Cell Biol. *165*, 709–721.
21. Hatten, M.E. (1985). Neuronal regulation of astroglial morphology and proliferation in vitro. J. Cell Biol. *100*, 384–396.
22. Inglis, P.N., Boroevich, K.A., and Leroux, M.R. (2006). Piecing together a ciliome. Trends Genet. *22*, 491–500.
23. Gherman, A., Davis, E.E., and Katsanis, N. (2006). The ciliary proteome database: An integrated community resource for the genetic and functional dissection of cilia. Nat. Genet. *38*, 961–962.
24. Efimenko, E., Bubb, K., Mak, H.Y., Holzman, T., Leroux, M.R., Ruvkun, G., Thomas, J.H., and Swoboda, P. (2005). Analysis of *xbx* genes in *C. elegans*. Development *132*, 1923–1934.
25. Blacque, O.E., Perens, E.A., Boroevich, K.A., Inglis, P.N., Li, C., Warner, A., Khattra, J., Holt, R.A., Ou, G., Mah, A.K., et al. (2005). Functional genomics of the cilium, a sensory organelle. Curr. Biol. *15*, 935–941.
26. Broadhead, R., Dawe, H.R., Farr, H., Griffiths, S., Hart, S.R., Portman, N., Shaw, M.K., Ginger, M.L., Gaskell, S.J., McKean, P.G., et al. (2006). Flagellar motility is required for the viability of the bloodstream trypanosome. Nature *440*, 224–227.
27. Andersen, J.S., Wilkinson, C.J., Mayor, T., Mortensen, P., Nigg, E.A., and Mann, M. (2003). Proteomic characterization of the human centrosome by protein correlation profiling. Nature *426*, 570–574.
28. Li, J.B., Gerdes, J.M., Haycraft, C.J., Fan, Y., Teslovich, T.M., May-Simera, H., Li, H., Blacque, O.E., Li, L., Leitch, C.C., et al. (2004). Comparative genomics identifies a flagellar and basal body proteome that includes the BBS5 human disease gene. Cell *117*, 541–552.
29. Avidor-Reiss, T., Maer, A.M., Koundakjian, E., Polyanovsky, A., Keil, T., Subramaniam, S., and Zuker, C.S. (2004). Decoding cilia function: Defining specialized genes required for compartmentalized cilia biogenesis. Cell *117*, 527–539.
30. Stolc, V., Samanta, M.P., Tongprasit, W., and Marshall, W.F. (2005). Genome-wide transcriptional analysis of flagellar regeneration in *Chlamydomonas reinhardtii* identifies orthologs of ciliary disease genes. Proc. Natl. Acad. Sci. USA *102*, 3703–3707.
31. Fan, Y., Esmail, M.A., Ansley, S.J., Blacque, O.E., Boroevich, K., Ross, A.J., Moore, S.J., Badano, J.L., May-Simera, H., Compton, D.S., et al. (2004). Mutations in a member of the Ras superfamily of small GTP-binding proteins causes Bardet-Biedl syndrome. Nat. Genet. *36*, 989–993.
32. Chiang, A.P., Nishimura, D., Searby, C., Elbedour, K., Carmi, R., Ferguson, A.L., Secrist, J., Braun, T., Casavant, T., Stone, E.M., et al. (2004). Comparative genomic analysis identifies an ADP-ribosylation factor-like gene as the cause of Bardet-Biedl syndrome (BBS3). Am. J. Hum. Genet. *75*, 475–484.
33. Collins, J.S., and Schwartz, C.E. (2002). Detecting polymorphisms and mutations in candidate genes. Am. J. Hum. Genet. *71*, 1251–1252.
34. Hanzal-Bayer, M., Renault, L., Roversi, P., Wittinghofer, A., and Hillig, R.C. (2002). The complex of Arl2-GTP and PDE delta: from structure to function. EMBO J. *21*, 2095–2106.
35. Vetter, I.R., and Wittinghofer, A. (2001). The guanine nucleotide-binding switch in three dimensions. Science *294*, 1299–1304.
36. Pasqualato, S., Menetrey, J., Franco, M., and Cherfils, J. (2001). The structural GDP/GTP cycle of human Arf6. EMBO Rep. *2*, 234–238.
37. Kelly, S.M., Jess, T.J., and Price, N.C. (2005). How to study proteins by circular dichroism. Biochim. Biophys. Acta *1751*, 119–139.
38. Zaki, M.S., Abdel-Aleem, A., Abdel-Salam, G., Marsh, S.E., Silhavy, J.L., Barkovich, A.J., Ross, M.E., Saleem, S.N., Dobyns, W.B., and Gleeson, J.G. (2008). The molar tooth sign: A new Joubert syndrome and related cerebellar disorders classification system tested in Egyptian families. Neurology *70*, 556–565.
39. Sun, Z., Amsterdam, A., Pazour, G.J., Cole, D.G., Miller, M.S., and Hopkins, N. (2004). A genetic screen in zebrafish identifies cilia genes as a principal cause of cystic kidney. Development *131*, 4085–4093.
40. Amsterdam, A., Burgess, S., Golling, G., Chen, W., Sun, Z., Townsend, K., Farrington, S., Haldi, M., and Hopkins, N. (1999). A large-scale insertional mutagenesis screen in zebrafish. Genes Dev. *13*, 2713–2724.
41. den Hollander, A.I., Koenekoop, R.K., Mohamed, M.D., Arts, H.H., Boldt, K., Towns, K.V., Sedmak, T., Beer, M., Nagel-Wolfrum, K., McKibbin, M., et al. (2007). Mutations in LCA5,

encoding the ciliary protein lebercilin, cause Leber congenital amaurosis. Nat. Genet. *39*, 889–895.
42. Zhao, Y., Hong, D.H., Pawlyk, B., Yue, G., Adamian, M., Grynberg, M., Godzik, A., and Li, T. (2003). The retinitis pigmentosa GTPase regulator (RPGR)- interacting protein: subserving RPGR function and participating in disk morphogenesis. Proc. Natl. Acad. Sci. USA *100*, 3965–3970.
43. Del Cerro, M.P., and Snider, R.S. (1969). The Purkinje cell cilium. Anat. Rec. *165*, 127–130.
44. Del Cerro, M.P., and Snider, R.S. (1972). Studies on the developing cerebellum. II. The ultrastructure of the external granular layer. J. Comp. Neurol. *144*, 131–164.
45. Bishop, G.A., Berbari, N.F., Lewis, J., and Mykytyn, K. (2007). Type III adenylyl cyclase localizes to primary cilia throughout the adult mouse brain. J. Comp. Neurol. *505*, 562–571.
46. Chizhikov, V.V., Davenport, J., Zhang, Q., Shih, E.K., Cabello, O.A., Fuchs, J.L., Yoder, B.K., and Millen, K.J. (2007). Cilia proteins control cerebellar morphogenesis by promoting expansion of the granule progenitor pool. J. Neurosci. *27*, 9780–9789.
47. Higginbotham, H., Bielas, S., Tanaka, T., and Gleeson, J.G. (2004). Transgenic mouse line with green-fluorescent protein-labeled Centrin 2 allows visualization of the centrosome in living cells. Transgenic Res. *13*, 155–164.
48. Burd, C.G., Strochlic, T.I., and Gangi Setty, S.R. (2004). Arf-like GTPases: Not so Arf-like after all. Trends Cell Biol. *14*, 687–694.
49. Gillingham, A.K., and Munro, S. (2007). The small G proteins of the Arf family and their regulators. Annu. Rev. Cell Dev. Biol. *23*, 579–611.
50. Brancati, F., Barrano, G., Silhavy, J.L., Marsh, S.E., Travaglini, L., Bielas, S.L., Amorini, M., Zablocka, D., Kayserili, H., Al-Gazali, L., et al. (2007). CEP290 mutations are frequently identified in the oculo-renal form of Joubert syndrome-related disorders. Am. J. Hum. Genet. *81*, 104–113.
51. Parisi, M.A., Doherty, D., Eckert, M.L., Shaw, D.W., Ozyurek, H., Aysun, S., Giray, O., Al Swaid, A., Al Shahwan, S., Dohayan, N., et al. (2006). AHI1 mutations cause both retinal dystrophy and renal cystic disease in Joubert syndrome. J. Med. Genet. *43*, 334–339.
52. Valente, E.M., Brancati, F., Silhavy, J.L., Castori, M., Marsh, S.E., Barrano, G., Bertini, E., Boltshauser, E., Zaki, M.S., Abdel-Aleem, A., et al. (2006). AHI1 gene mutations cause specific forms of Joubert syndrome-related disorders. Ann. Neurol. *59*, 527–534.
53. Keeler, L.C., Marsh, S.E., Leeflang, E.P., Woods, C.G., Sztriha, L., Al-Gazali, L., Gururaj, A., and Gleeson, J.G. (2003). Linkage analysis in families with Joubert syndrome plus oculo-renal involvement identifies the CORS2 locus on chromosome 11p12-q13.3. Am. J. Hum. Genet. *73*, 656–662.
54. Valente, E.M., Salpietro, D.C., Brancati, F., Bertini, E., Galluccio, T., Tortorella, G., Briuglia, S., and Dallapiccola, B. (2003). Description, nomenclature, and mapping of a novel cerebello-renal syndrome with the molar tooth malformation. Am. J. Hum. Genet. *73*, 663–670.
55. Saar, K., Al-Gazali, L., Sztriha, L., Rueschendorf, F., Nur, E.K.M., Reis, A., and Bayoumi, R. (1999). Homozygosity mapping in families with Joubert syndrome identifies a locus on chromosome 9q34.3 and evidence for genetic heterogeneity. Am. J. Hum. Genet. *65*, 1666–1671.
56. Valente, E.M., Marsh, S.E., Castori, M., Dixon-Salazar, T., Bertini, E., Al-Gazali, L., Messer, J., Barbot, C., Woods, C.G., Boltshauser, E., et al. (2005). Distinguishing the four genetic causes of Joubert syndrome-related disorders. Ann. Neurol. *57*, 513–519.
57. Schrick, J.J., Vogel, P., Abuin, A., Hampton, B., and Rice, D.S. (2006). ADP-ribosylation factor-like 3 is involved in kidney and photoreceptor development. Am. J. Pathol. *168*, 1288–1298.
58. Wechsler-Reya, R.J., and Scott, M.P. (1999). Control of neuronal precursor proliferation in the cerebellum by Sonic Hedgehog. Neuron *22*, 103–114.
59. Lewis, P.M., Gritli-Linde, A., Smeyne, R., Kottmann, A., and McMahon, A.P. (2004). Sonic hedgehog signaling is required for expansion of granule neuron precursors and patterning of the mouse cerebellum. Dev. Biol. *270*, 393–410.
60. Spassky, N., Han, Y.G., Aguilar, A., Strehl, L., Besse, L., Laclef, C., Romaguera Ros, M., Garcia-Verdugo, J.M., and Alvarez-Buylla, A. (2008). Primary cilia are required for cerebellar development and Shh-dependent expansion of progenitor pool. Dev. Biol. *317*, 246–259.